Dissimilar laser brazing of h-BN and WC-Co alloy in Ar atmosphere without evacuation process

Y Sechi[1] , K Nagatsuka[2] and K Nakata[3]
[1] Kagoshima Prefectural Institute of Industrial Technology, 1445-1 Oda, Hayato-cho, Kirishima, Kagoshima 899-5105, Japan
[2] Graduate School of Engineering, Osaka University, 2-1 Yamadaoka, Suita, Osaka 565-0871, Japan
[3] Joining and Welding Research Institute, Osaka University, 11-1 Mihogaoka, Ibaraki, Osaka 567-0067, Japan

E-mail: sechi@kagoshima-it.go.jp

Abstract. Laser brazing with Ti as an active element in Ag-Cu alloy braze metal has been successfully applied to dissimilar joining of h-BN and WC-Co alloy in Ar (99.999% purity) gas flow atmosphere without any evacuation process. Good wettability of the braze metal with h-BN and WC-Co alloy were confirmed by the observation and structural analysis of the interface by electron probe micro-analysis and scanning acoustic microscopy. The oxidation of titanium was not observed and this showed that the laser brazing with titanium as an active element in braze metal could be performed even in an Ar gas flow atmosphere without an evacuation process using a high-vacuum furnace.

1. Introduction

The brazing process is used in many industrial fields for developing engineering structures and electronic devices [1-13]. This process has several advantages making it suitable for use in joining dissimilar materials and materials which are difficult to connect precisely; further, this process can be efficiently applied to the mass production of structures and devices. For the application of ceramic materials, it is frequently required that a ceramic material be bonded to metals. Moreover, the development of high-functionality products in recent years has led to a demand for a new joining process that can join different materials. However, certain problems are encountered while meeting the above requirements, such as the formation of joint defects due to thermal stress in the joint field and material deterioration due to heating in the brazing process.

Boron nitride has various functional characteristics. Especially, h-BN has a good thermal resistibility and solid-lubrication [14]. Meanwhile, it is difficult to braze h-BN to another material because of its low wettability. As a result, it is difficult to braze hexagonal boron nitride ceramics to other materials. Because wettability of a material affects joining characteristics, it is speculated that brazing of hexagonal boron nitride ceramics may be suitable to demonstrate laser brazing of dissimilar materials such as ceramics and a metal.

In general, the thermal expansion coefficient of a metal is higher than that of ceramics; this may result in the generation of a large thermal stress at the brazing joint, which leads to the formation of defects at the interface [15]. Tungsten carbide / cobalt alloy made by powder metallurgy has a low thermal expansion coefficient and high rigidity, which is a good complement as a

structural material to ceramics. However, only a few studies have focused on the joining of boron nitride and tungsten carbide alloy or other metals [5, 8, 10] by brazing in a furnace that needs a long heating time.

Among brazing processes [16], laser brazing [10, 11, 13, 17-30] has good characteristics for a dissimilar joining process because of the possibility of short heating time and small heating area, and suppression of damage to the base materials without a furnace, in comparison with conventional furnace brazing.

Recently, laser brazing with the addition of Ti as an active element in Ag-Cu alloy braze metal has been successfully applied to dissimilar joining of h-BN and WC-Co alloy after the evacuation on the order of 10^{-1} Pa and Ar (99.999% purity) substitution to avoid oxidation of the active element of Ti [12], but a more simplified method without evacuation is needed for the practical use of dissimilar laser brazing. So this study describes the dissimilar laser brazing of h-BN and WC-Co alloy without an evacuation process and the characteristics of a dissimilar joint, and in order to investigate the characteristics of the dissimilar joint, cross-sectional observation, elemental and structural analyses of the joint interface, adhesion evaluation, and shear strength measurement were performed.

2. Experimental procedures

Commercially available tungsten carbide equivalent material classified with ISO K10 grade and high-purity h-BN made by the hot pressing method without using sintering additives were used in this work. Silver-copper-titanium alloy braze metal sheet included Ti as a major active ingredient for direct ceramic brazing with a thickness of 0.1 mm. Nominal compositions and properties are summarized in Tables 1 and 2. The size of the braze metal sheet was determined to cover 80% of the joint area of h-BN so that the melted braze metal would not flow out of the joint. Before brazing, the h-BN block, braze metal and tungsten carbide plate were degreased by ultrasonic agitation for 10 min in acetone and dried in air. Sample configuration was a top hat shape. A braze metal sheet was sandwiched with an h-BN block from the top and a tungsten carbide plate from the bottom in a vacuum chamber. A low pressure of 1.2 MPa was applied to prevent the workpiece from moving when the braze metal sheet was melted, and no gap adjustments for the joint were performed. A chamber with a 100 mm diameter was used in the brazing experiments, which had inner volume 145 ml. To avoid the oxidation of Ti, 99.999% purity Ar was flowed during laser brazing at a rate of 10 L/min without evacuation of the chamber.

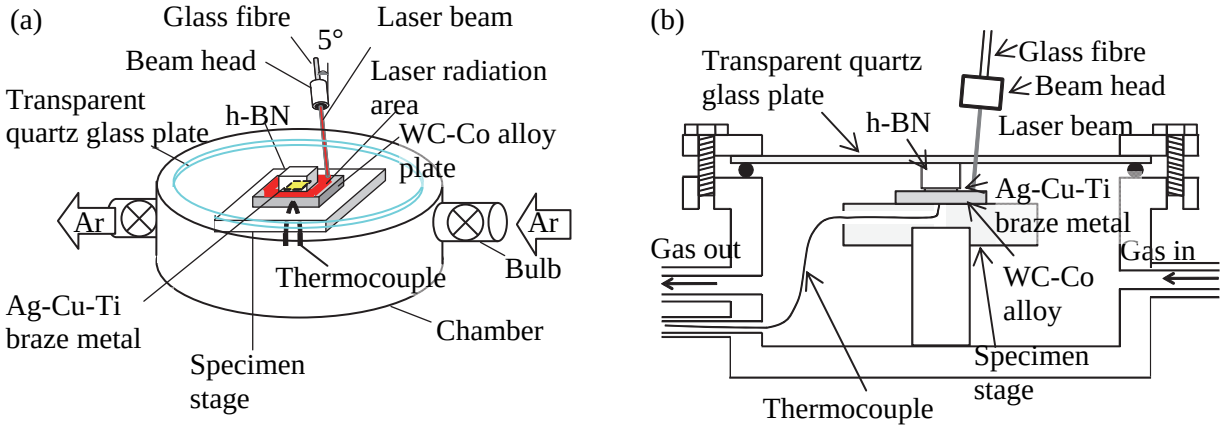

(a) perspective illustration (b) cross-sectional illustration

Figure 1. Schematic diagram of laser brazing.

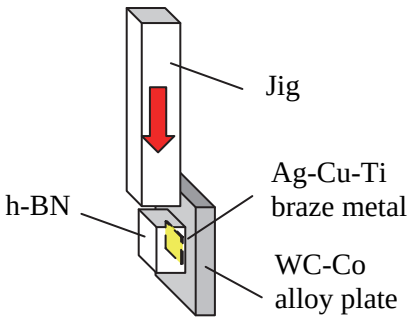

Figure 2. Schematic diagram of shear strength test.

Table 1. Materials used in this work.

Material	Nominal composition (mass %)	Density ($\times 10^3$ kg / m^3)	Relative Density (%)	Size (mm)
Tungsten Carbide	WC: 94, Co: 6	14.9	-	10*10*2
h-BN	h-BN > 99.993	1.93	82.5	5*5*3.5

Table 2. Chemical composition of Ag-Cu-Ti alloy braze metal.

Elements (mass %)		
Ag	Cu	Ti
70.2	bal.	1.7

Table 3. Laser heating condition.

Pulsed YAG Average Output (kW)		0.134
Pulsed YAG wave length (nm)		1064
CW LD Output (kW)		0.02
CW LD wave length (nm)		808
Pulse frequency (Hz)		100
Scanning speed (mm/s)	(1^{st} run)	0.6
	(2^{nd} run)	1.0
	(3^{rd} run)	1.0
	(4^{th} run)	1.0
Laser beam diameter (mm)		0.5

The setup of laser brazing was as shown in Figure 1. In (a), a perspective illustration is shown, and in (b), a cross-sectional illustration is shown to describe the schematic diagram of laser brazing. The sample was located in a small vacuum chamber. The topside of the specimen was covered with a transparent quartz glass plate, which also acted to fix the specimen. The generated YAG and LD lasers were transferred with an optical fibre to the laser head unit and radiated through the transparent quartz glass plate to the topside of the tungsten carbide plate, with a radiation angle of 85°. Laser scanning of the tungsten carbide substrate was performed around the h-BN block. The laser brazing condition is summarized in Table 3. The scanning speed of laser was 0.6 mm/s on the first run and 1.0 mm/s on the

second run to the fourth run in order to heat the specimen efficiently in a circular manner. In this study, the laser scanning was performed on the tungsten carbide substrate around the h-BN block. Temperature during laser brazing was monitored at the bottom of the tungsten carbide plate using a thermocouple. Some of the samples were subsequently cross sectioned by a low-speed diamond saw with water cooling and mounted by epoxy resin, curing at room temperature for about 8-10 h, ground using SiC paper #120-#1200, and polished by 3 to 1 μm polycrystalline diamond to provide microstructural information. Cross-sectional observation and elemental analysis of the interface were performed using an electron probe micro-analyzer (JEOL Co. Ltd. JXA-8230) and an X-ray diffractometer (Bruker AXS Co. Ltd. D8: Co Kα). The diameter of the collimator was 50 μm, to determine crystallographic phase of the micro-region. Interfacial observation and estimation of the interface area were performed using a scanning acoustic microscope (Hitachi Kenki FineTech Co., Ltd. HSAM220), which can observe interfacial structure using ultrasonic echo radiated from the probe in a water tank. Some of the samples were placed in a shearing jig as shown in Figure 2 and stressed to destruction in a precision universal tester (Shimadzu Cooperation Autograph AGS-5kNB) operating at a crosshead speed of 0.5 mm/min. In order to compensate the effect of interfacial area on the shear strength test, shear strength was calculated from the maximum load divided by the interface area estimated from scanning acoustic microscopy, and its average shear strength was calculated using the Weibull distribution function [31, 32]:

$$\ln \ln(1-F)^{-1} = m \ln\sigma - m \ln \sigma_0, \quad (1)$$

where F is the cumulative failure probability, m is the Weibull modulus, and σ_0 is the characteristic strength. In this paper, the median rank method was used for computing cumulative failure probability F in Eq. (1) because of its good reliability despite the small number of samples:

$$F = (i - 0.3) / (n + 0.4), \quad (2)$$

where i is the rank of the observation and n is the number of samples. Average shear strength is as follows:

$$\mu = \sigma_0 \Gamma(1+1 / m), \quad (3)$$

where the Γ function is expressed as follows.

$$\Gamma(x) = \int_0^\infty e^{-t} t^{x-1} dt \quad (x > 0). \quad (4)$$

3. Results

3.1. Heating profile and appearance of a specimen

Figure 3 shows the typical profile of the bottom temperature of the WC-Co plate during laser brazing joining. The increase of temperature continued in approximate proportion to the gradient until irradiation of the laser on the fourth side. The maximum bottom temperature was around 900 K. After the heating, the bottom temperature decreased quickly to 620 K within 25 sec from the end of the fourth run of heating.

The maximum bottom temperature of the WC-Co alloy in this case was about 70 K lower than that of the case at the Ar gas flow rate of 5 L/min with an evacuation process [12], but both temperature profiles showed a similar trend.

Figure 4 (a) and (b) shows the appearance of the specimen and the scanning acoustic microscopy image at the interface of h-BN / Ag-Cu-Ti braze metal / WC-Co, respectively, after laser brazing. In (a), the white part of the square in the centre is an h-BN block, and the peripheral metallic lustre part is WC-Co. At the right side in (a), a Ag-Cu-Ti braze metal lump, which occasionally flowed out from the

interface between h-BN and WC-Co, as indicated by a white arrow can be seen, and its colour kept a metallic lustre, which showed that a large amount of titanium oxide did not exist at the surface of the braze metal. The black area in the centre of (b) is Ag-Cu-Ti braze metal which was melted at the joint interface and no void was observed in the joint interface.

Figure 5 shows a typical cross-sectional SEM image at the interface of h-BN / Ag-Cu-Ti braze metal / WC-Co after laser brazing. The upper right side is h-BN and lower area is the WC-Co alloy plate. The gray layer between h-BN and WC-Co is Ag-Cu-Ti braze metal. As an active element in Ag-Cu alloy braze metal, Ti reacted with N in h-BN, and a continuous TiN layer was formed at the interface, which improved the wettability between ceramics and braze metal. Also, Ti reacted with C in WC-Co, and a continuous reaction layer was formed at the interface between braze metal and WC-Co. These results reveal a similar tendency to the former study with evacuation process [12]. Therefore, these observations are addressed in the former study [12].

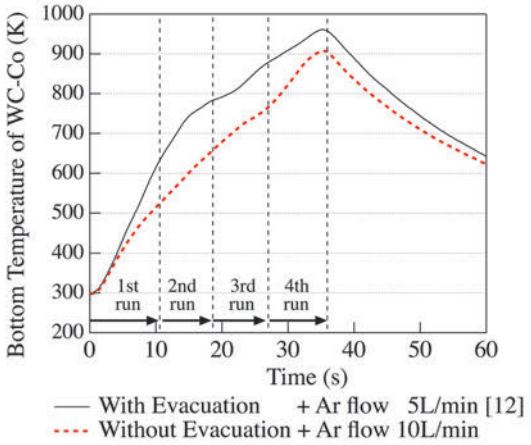

Figure 3. Heating profile of the bottom temperature profile of the WC–Co plate during laser brazing.

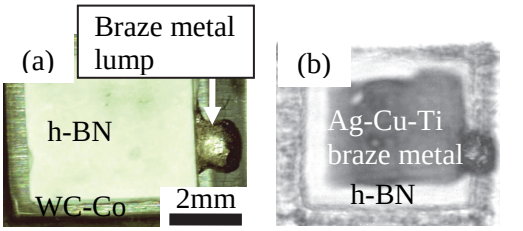

(a) Appearance of a brazed specimen

(b) Scanning acoustic microscopy image

Figure 4. Appearance of a laser brazed specimen and interface observation of a h-BN / Ag-Cu-Ti braze metal / WC-Co interface using scanning acoustic microscopy.

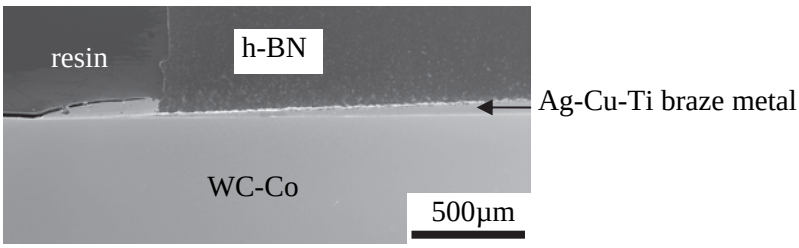

Figure 5. Cross-sectional SEM image of the specimen.

3.2. The surface condition of Ag-Cu-Ti braze metal

Figure 6 shows cross-sectional SEM observation of an edge of the h-BN / Ag-Cu-Ti braze metal interface and its map analysis using electron probe micro-analysis. In (a), the upper left area is h-BN as indicated, the lower whitish area shows the Ag-Cu-Ti braze metal, the upper right area is epoxy resin which is used to mount the specimen and there is a space between the Ag-Cu-Ti braze metal and epoxy resin because of the shrinkage of the curing epoxy resin. The resin side of the Ag-Cu-Ti braze metal corresponds to the surface of the melted braze metal, which overflowed from the h-BN/WC-Co interface and was exposed to the Ar atmosphere. In (b), the distribution of oxygen was limited to the epoxy resin area and was not observed in the Ag-Cu-Ti braze metal. In (c) and (d), the distributions of silver and copper were the same as that of the braze metal area, as shown in the SEM image. The distribution of titanium is shown in (e). In (f) and (g), the distributions of boron and nitrogen were the same as that of the h-BN area. In (e), most of the titanium existed at the interface between the h-BN and Ag-Cu-Ti braze metal, and overlap of the distribution of nitrogen and titanium was observed, as shown in (g), which suggested the formation of a reacted layer of Ti-N intermetallic compound [5]; and the rest of the titanium was in the bulk of the braze metal, which overlapped the concentration of copper shown in (d). In the high-concentration regions of titanium and copper, the concentration of silver was low in contrast with titanium and copper. These results showed a similar tendency to that of the former study with evacuation [12]. From (b) and (e), the distributions of oxygen and titanium were not overlapped, which was apparently distinguished due to the existence of the space between the Ag-Cu-Ti braze metal and resin. These facts show that the oxidation layer was not observed at the surface of the melted braze metal.

In (h), the concentration of tungsten was low, and its detection was at background level. In (i), the distribution of carbon was limited to the epoxy resin area. In (j), the concentration of cobalt was low, and its detection was at background level in the same way as tungsten.

Figure 7 shows surface SEM observation of Ag-Cu-Ti braze metal lump and its map analysis using electron probe micro-analysis. In (a), small white spots are considered as contamination on the surface of Ag-Cu-Ti braze metal from their forms. In (b), the concentration of oxygen was low and its detection was at background level, and a significant concentration of oxygen was not observed. In (c), (d) and (e), the distribution of silver, copper and titanium, which were elements of braze metal, were the same as that of the braze metal area as shown in the SEM image of (a). In the high-concentration regions of titanium and copper, the concentration of silver was low in contrast with titanium and copper. In (f) and (g), the concentrations of boron and nitrogen were low and their distributions were restricted to small white spots which were considered as contamination on the surface. In (h), (i) and (j), the concentrations of tungsten, carbon and cobalt, which were elements of WC-Co, were low and their detection was at background level.

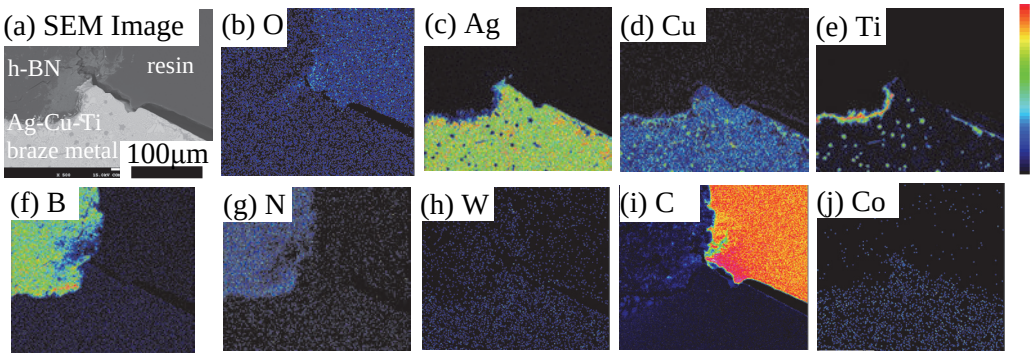

Figure 6. Map analysis of h-BN/Ag-Cu-Ti braze metal interface (at the edge).

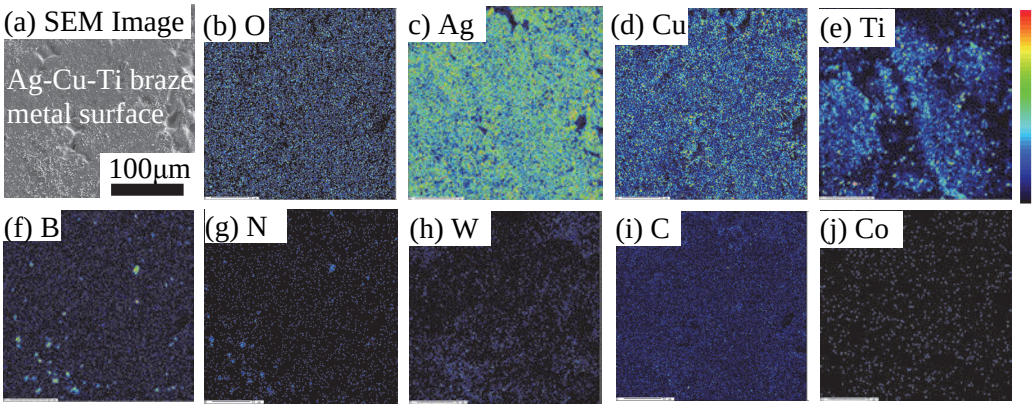

Figure 7. Map analysis of Ag-Cu-Ti braze metal surface (at the braze metal lump).

3.3. The interface condition between h-BN and Ag-Cu-Ti braze metal

Figure 8 shows cross-sectional SEM observation and its map analysis of the central area of an h-BN / Ag-Cu-Ti braze metal interface. In Figure 8 (a), the upper area is h-BN as indicated, and the lower gray area shows Ag-Cu-Ti braze metal. In (b), oxygen was not observed at the interface. Silver near the interface in the same area of (a) is shown in (c) and also copper is shown in (d). In (e), the distribution of titanium was concentrated at the interface. In (f) and (g), the distributions of boron and nitrogen were the same as that of h-BN area, as shown in the SEM image of (a). From these element distributions, titanium concentration near the interface was apparently observed, of which the thickness was about 2-5 μm. The interface between h-BN and Ag-Cu-Ti was very complicated. It is presumed that the molten Ag-Cu-Ti braze metal infiltrated into open pores of the h-BN surface. These results showed a similar tendency to that in the former study with evacuation [12]. In (h), (i) and (j), the distributions of tungsten, carbon and cobalt, which are elements of WC-Co, are shown. Concentrations of tungsten and cobalt were low, at background level. In (i), the concentration of carbon was observed in the ragged area of h-BN as shown in the SEM image of (a), which was considered to be contamination remaining from the polishing material. In (j), the concentration of cobalt was low, at background level.

Figure 9 shows XRD profiles of the samples at the interface of the h-BN / Ag-Cu-Ti braze metal without evacuation and with evacuation [12] in the central area of the interface. Among the strong peaks of h-BN, WC-Co and silver, which resulted from bulk ceramics, WC-Co and braze metal elements, respectively, some peaks from titanium nitride were found to exist at the interface. These weak peaks were indexed as TiN [2, 6, 10] in both cases. Oxide peaks such as TiO_2 were not observed even in the case without evacuation.

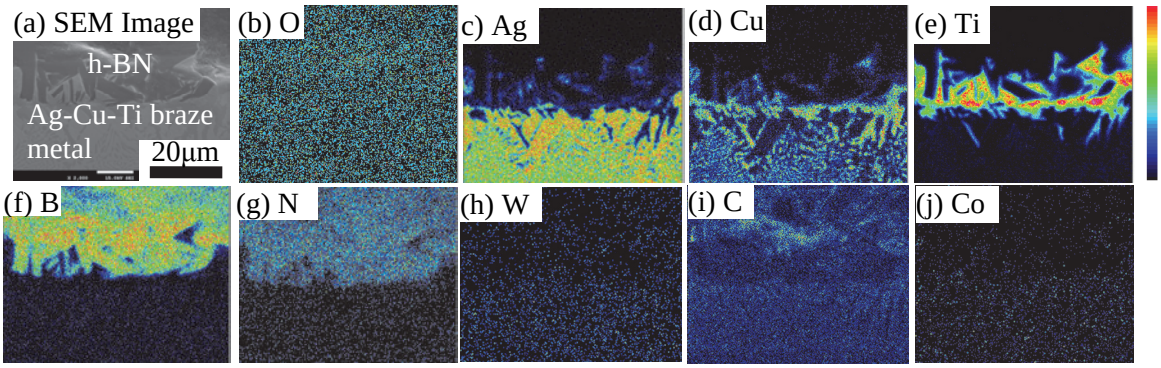

Figure 8. Map analysis of an h-BN/Ag-Cu-Ti braze metal interface (at the central area).

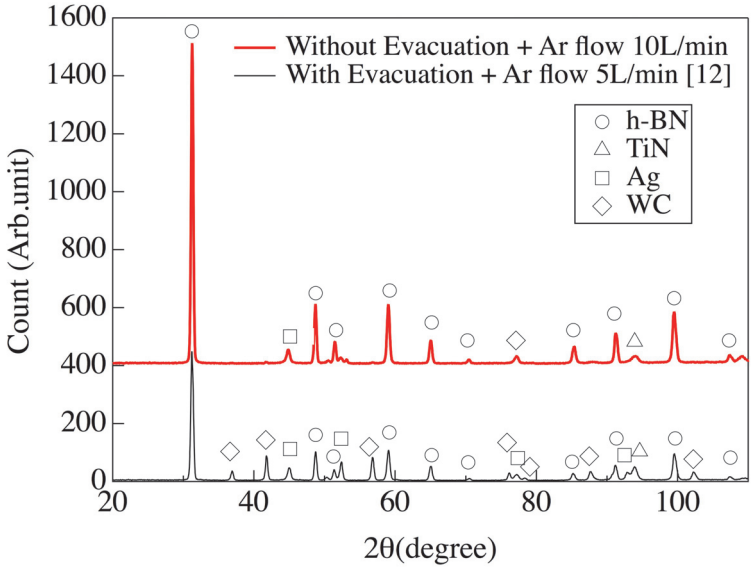

Figure 9. XRD profile of the h-BN/Ag-Cu-Ti braze metal interface.

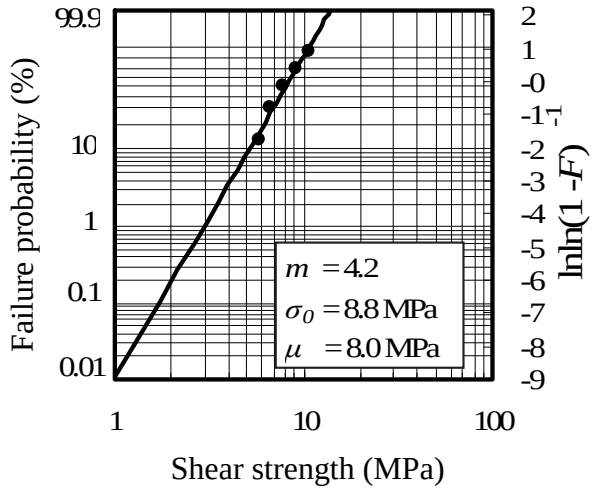

Figure 10. The Weibull distribution of shear strength test.

3.4. Shear strength test

After cross-sectional and non-destructive examinations, a shear strength test of the dissimilar joint was performed. Figure 10 shows the Weibull distribution of shear strength tests of h-BN / Ag-Cu-Ti braze metal and h-BN, which was plotted using the median rank method. In all tests, fracture occurred at h-BN side of the specimen near the interface. The difference between the maximum and minimum shear strengths was about 4-5 MPa. The distributions of shear strength were spread widely and could be approximated by the line formula as shown. The average shear strength μ was 8.0 MPa, which showed similar strength to that obtained by supplying Ar gas after evacuating the chamber before brazing [12].

4. Discussion

As shown in Figure 3, the maximum bottom temperature of WC-Co alloy in this case was about 70 K lower than for the case with an evacuation process of the chamber before brazing [12]. It is assumed that this decrease in temperature results from the difference in cooling effect with the flow rate of Ar. However, Ag-Cu-Ti braze metal was melted, and a reaction layer at the interface was formed as shown in Figures 4, 6 and 8. These facts indicate that the brazing condition in this study is sufficient to melt the Ag-Cu-Ti braze metal and make the joint.

Figure 4 shows that the Ag-Cu-Ti braze metal, which flowed out from the interface between h-BN and WC-Co, had a metallic lustre. This fact shows that a large amount of titanium oxide did not exist at the surface of the Ag-Cu-Ti braze metal, even when only Ar gas was supplied at a flow rate of 10 L/min without evacuating the chamber before brazing.

From Figure 6 (a), the upper right area of Ag-Cu-Ti braze metal was exposed to Ar gas. If the remaining amount of oxygen in Ar gas flow atmosphere was sufficient to react with titanium in the braze metal, titanium oxide would be formed, but the distribution of oxygen in (b) showed that the oxidation layer was not observed at the surface of the braze metal. In addition, from Figure 7 (b), the concentration of oxygen was low and its detection was at background level, and a significant concentration of oxygen was not observed in the surface elemental analysis. Thus, it is considered that the oxidation layer at the surface of the braze metal over sub-micrometre order, which is the minimum limit of detection of EPMA, was not observed. In the conventional dissimilar brazing process, a vacuum furnace is commonly used to avoid oxidation of Ag-Cu-Ti braze metal during a long brazing period. In contrast, the laser brazing process enabled the realization of a good braze metal joint without oxidation by supplying only Ar gas at a flow rate of 10 L/min, even without evacuating the chamber before brazing.

In Figures 6 and 8, the concentrations of tungsten, carbon and cobalt were low and it is considered that they have little or no effect on the interfacial reaction compared to the former study [12]. In Figure 7, the concentrations of tungsten, carbon and cobalt were low and their detection was at background level, and these concentrations are considered that they have little or no effect on the surface reaction of Ag-Cu-Ti braze metal.

Figures 8 to 10 indicate that the brazing behaviour [2, 34, 35] and the average shear strength were similar to those in the former study [12] even when supplying only Ar gas at a flow rate of 10 L/min without any evacuation process of the chamber before brazing.

5. Conclusions

(1) The laser brazing of h-BN and WC-Co alloy using Ag-Cu-Ti braze metal as an active element of titanium could be achieved only in a high-purity Ar gas flow atmosphere in a chamber without any evacuation process.
(2) Oxidation of titanium was not observed, and titanium existed as Cu-Ti composite in Ag-Cu-Ti braze metal near the edge of the braze metal.
(3) Average shear strength calculated from the interface area was 8.0 MPa, which showed similar strength to that obtained by using an evacuation process.

Acknowledgements

This work was supported by the Joint Research System of the Joining and Welding Research Institute, Osaka University.

References

[1] Nakao Y, Nishimoto K and Saida K 1989 *Trans of J.W.S.* **20** 66-76
[2] Nicholas M G, Mortimer D A, Jones L M and Crispin R M 1990 *J. Mat. Sci*. **25** 2679-89
[3] Nakao Y, Nishimoto K and Saida K 1990 *ISIJ Int*. **30** 1142-50
[4] Murakawa M and Takeuchi S 1991 *Mater. Sci. Eng.* A **140** 759-63
[5] Chattopadhyay A K and Hintermann H E 1993 *J. Mat. Sci.* **28** 5887-93
[6] Peteves S D 1996 *Ceram. Int.* **22** 527-33
[7] Fernandes A J S, Fonseca M J, Costa F M, Silva R F and Nazare M H 1999 *Dia. Rel. Mat.* **8** 855-8
[8] Felba J, Friedel KP, Krull P, Pobol I L and Wohlfahrt H 2001 *Vac*. **62** 171-80
[9] Huang S F, Tsai H L and Lin S T 2004 *Mater. Chem. Phys.* **84** 251-8
[10] Sechi Y, Takezaki A, Tsumura T and Nakata K 2008 *Smart Process Tech*. **2** 27-30
[11] Rohde M, Suedmeyer I, Urbanek A and Torge M 2009 *Ceram. Int*. **35** 333-7
[12] Sechi Y, Tsumura T and Nakata K 2010 *Materials and Design* **31** 2071-7
[13] Suedmeyer I, Hettesheimer T and Rohde M 2010 *Ceram. Int*. **36** 1083-90
[14] Biddulph R H 1985 *Proceedings of the 1st Europian Symposium on Engineering Ceramics* p.45-61
[15] Wlosinski W 1985 *Fueg. Keram. Gla. Met*. p.22-36
[16] Jenney C L, O'Brien 2001 *A Welding Handbook* Vol. I. (American Welding Society)
[17] Witherell C E and Ramos T J 1980 *Weld J*. **59** 267S-277S
[18] Hanebuth H, Hoffmann P and Geiger M 1994 *Proc. SPIE Int. Soc. Opt. Eng.* 2207: 146-153
[19] Whitehead D G and Foster R J 1995 *Assem. Auto.* **15** 17-19
[20] Dave V R, Carpenter R W, Milewski J O, and Christensen D T 2001 *Weld. J*. **80** 142.S-147.S
[21] Markovits T, Takacs J, Lovas A and Belt J 2003 *J. Mater. Process. Technol*. **143/144** 651-5
[22] Vollertsen F and Grupp M 2005 *Steel Res. Int*. **76** 240-4
[23] Saida K, Song W and Nishimoto K. 2005 *Sci. Tech. Weld. Join*. **10** 227-35
[24] Mathieu A, Cicala E, Matteie S, Gewvey D, Pontevicci S and Viala J C 2006 *Mater. Sci. Eng.* A **435/436** 19-28
[25] Li M G, Sun D Q, Qiu X M, Sun D X and Yin S Q 2006 *Mater. Sci. Eng*. A **424** 17-22
[26] Mathieu A, Matteie S, Grevey D, Deschamps A and Martin B 2006 *NDT E Int*. **39** 272-6
[27] Saida K, Song W and Nishimoto K 2006 *Sci. Tech. Weld. Join*. **11** 694-700
[28] Saida K, Song W and Nishimoto K 2007 *Design Int. Str. Adv. Mat. Join. Sol. Sta. Phen.* (Part B) **127** 301-6
[29] Takemoto T, Kawahito Y, Nishikawa H, Katayama S and Kimura S 2008 *J. Lig. Met. Weld. Cons*. **46** 300-8
[30] Saida K, Song W and Nishimoto K 2008 *Mat. Sci. For*. **580/582** 271-4
[31] Weibull W 1951 *J. Appl. Mech*. **18** 293-7
[32] Stanley P, Fessler H and Sivill A D 1973 *Proc. Brit. Ceram. soc*. **22** 453-87
[33] Chattopadhyay A K and Hintermann H E 1993 *J. Mat. Sci*. **28** 5887-93
[34] Benko E 1995 *Ceram. Int.* **21** 303-7
[35] Benko E, Bielanska E, Perevertelio V M and Loginova O B 1997 *Dia. Rel. Mat*. **6** 931-34